Contributions to Geophysics and Geodesy Vol. 56/1, 2026 (39–64)

Potential along a pipeline during geomagnetic storms and the geoelectric coast effect

Giovanni LUCCA*

Independent Researcher, Piacenza, Italy

Abstract: The paper proposes a calculation method for assessing the potential along a pipeline located near a coastline, due to the geomagnetic induction occurring during geomagnetic storms. The algorithm is based on the generalised thin sheet model to describe the inducing geoelectric field and on the transmission line model with lumped parameters to describe the pipeline under the influence of the geoelectric field, which is supposed to have a generic polarisation. In particular, the proposed calculation method allows for the assessment of the potential profile that can be generated along the pipeline and for the identification of the zones that are more exposed to the occurrence of high electric potentials. We remind that the overpotentials generated along the infrastructure can interfere with the pipeline cathodic protection and electrical survey apparatuses, affecting their correct functioning and so increasing the corrosion risk. Therefore, this model can be an aid, also at the design stage of a new infrastructure, able to individuate the riskiest zones along the pipeline layout, subjected to the highest potentials thus allowing to minimise the threaten represented by geomagnetic storms. The peculiarity and novelty of the paper, different from previous works, is the consideration of the geoelectric coast effect in the assessment of the potential profile along the pipeline route using an approach based on the generalised thin sheet model under a generic state of polarisation of the inducing geomagnetic field.

Key words: geomagnetic storms, telluric currents, geomagnetically induced currents, pipelines, geoelectric coast effect

1. Introduction

The natural time variations of the terrestrial geomagnetic field generate electric fields in the ground, driving electric currents generally known as telluric currents. This phenomenon is strongly enhanced during geomagnetic storms that occur when an intense solar wind interacts with the Earth's magnetosphere and ionosphere, generating, at ground level, geoelectric fields that may reach, at high latitudes, magnitudes of some V/km.

Ground-based technological infrastructures such as power lines, pipelines,

*corresponding author, e-mail: vanni.luccapc@gmail.com

doi: 10.31577/congeo.2026.56.1.3

metallic telecommunication cables, and railway lines are influenced by the above mentioned geoelectric fields (*Boteler, 2003; Pilipenko, 2021*), which drive potentials and currents in those technological systems with associated risk of damages and/or malfunctioning; as a final result, partial or total losses of service to the influenced infrastructure can occur.

In this paper, we focus on pipelines. Therefore, to understand the possible dangerous effects produced on these structures by geomagnetic storms, it is useful to previously and shortly recall the measures adopted to protect steel pipes buried in the ground against corrosion that naturally develops when the pipe metal is in contact with the soil.

The first protection means is the plastic coating (typically polyethylene) that covers the pipe surface with the purpose of insulating it from the ground to avoid any electrochemical reaction between the metal and the soil that leads to corrosion.

Nevertheless, this insulating barrier is never perfect due to the presence of small holes and ruptures in the pipe coating that are produced during fabrication, transportation and installation of the pipe itself; additionally, these defects may appear during the pipeline life due to a normal degradation process of the coating itself (*Lucca, 2016*).

At the location of these small holes in the coating, the pipe is in contact with the soil, and the corrosion process may occur provided that the pipe-to-soil potential (PSP) is positive. For such a reason, it is necessary to adopt a second protection means represented by the cathodic protection (CP); it consists in maintaining the PSP sufficiently negative (typically in the range $[-1.2\,\mathrm{V},\ -0.85\,\mathrm{V}]$) so that any current flow from the pipe to the soil is prevented and the corrosion process cannot start.

It is also important to note that if the PSP is lower than $-1.2\,\mathrm{V}$ the insulating coating can disbond from the steel pipe, and soil water can come into contact with the metal, leading to corrosion (*von Baeckmann et al., 1997*). On the other hand, if the PSP is higher than $-0.85\,\mathrm{V}$ for long duration, the pipe may corrode. Thus, it is important that CP operates in the abovementioned range.

During geomagnetic storms, the PSP can present significant fluctuations well beyond the range $[-1.2\,\mathrm{V},\ -0.85\,\mathrm{V}]$ so that the CP system may be unable to correctly operate, with a consequent increased risk of pipe corrosion and coating disbonding.

In light of these observations, we understand how useful it can be to have available calculation models that allow us to evaluate geomagnetically induced currents (GICs) and potential along the pipeline.

One of the first works dates back to 1998 (*Boteler and Seager, 1998*); the basic idea was to model a pipeline as a transmission line circuit with distributed sources (DSTL) and apply the so called "Telegrapher's equations" that are employed to study electromagnetic interference in a wide range of technological systems; the results of the calculations are well fitted with field measurements. In the following years, the model was refined to consider bendings, discontinuities, and secondary branches along the pipeline (*Boteler, 2000; Pulkkinen et al., 2001*).

A further step was introduced by *Boteler (2013)* and *Boteler et al. (2013)* by modelling the transmission line circuit, representing the pipeline, using a chain of Pi circuits that can be transformed into a nodal network.

In the last years, *de Moraes et al. (2020)* evaluated, using the DSLT model, the possible corrosion enhancement due to the geomagnetic storm of March 17, 2015, on the Bolivia-Brazil gas pipeline. The same model has been used by *Trichtchenko et al. (2023)* for studies concerning the effects of strong geomagnetic activity (in 2003 and 2004) on Australian and European pipelines. *Divett et al. (2023)* applied the nodal network theory to study the influence of geomagnetic storms on the main gas pipeline network located in the North Island of New Zealand.

An important point to be considered in PSP evaluation is the proximity of the pipeline to a coast because, as quoted in the literature, all ground-based technological infrastructures not far from a coastline are influenced by this factor (*Boteler, 1994; Dong et al., 2013*).

Nevertheless, little attention has been paid, in specific literature, to the geoelectric coast effect on pipelines. An exception is given by *Liu et al. (2022)* and *Liu (2024)* that studied the influence of the coast effect on a pipe network by representing the earth and sea structure using the block and thin shell models introduced by *Liu et al. (2019a)* and *Liu et al. (2019b)*.

In the present paper, we also want to study the geomagnetic influence on a pipeline in the presence of the coast effect, but we shall adopt a different earth and sea representation based on the generalised thin sheet model, that, differently from the previous ones, allows to take into account the earth stratification.

The generalised thin sheet model is an extension of the thin sheet model involving a single thin surface layer (see for example *McKay (2003)* that adopted it to study the GIC in the Scottish power electricity network). It was first introduced by *Ranganayaki and Madden (1980)* and consists of an approximate analytical method for the calculation of the geoelectric field that can be applied for two-dimensional problems. Different from the thin sheet model, the generalised thin sheet model involves a surface double layer. Further information about it, for the case of H polarisation of the inducing geomagnetic can be found in the PRCI Report (*Gummow et al., 2002*) and in the paper by *Wang et al. (2023)*, while *Lucca (2024b)* extended the formulation to the generic case of mixt H and E polarisation.

In the present work, we shall apply the latter and more general approach concerning the polarisation of the inducing geomagnetic field because this parameter plays a fundamental role in evaluating the PSP along a pipeline under the influence of a geomagnetic storm. As far as the representation of the pipeline is concerned, we shall apply the transmission line circuit with lumped element that is equivalent to the representation given by *Boteler (2013)* and by *Boteler et al. (2013)*.

2. Basic hypotheses of the calculation method

This section introduces the basic definitions and fundamental hypotheses on which the calculation method is grounded.

Let us start by defining E and H polarisation; to this purpose, let us consider the source geomagnetic field represented by a plane wave normally incident to the xy plane representing the air-land/sea interface. We have E/H polarisation when the incident magnetic field is perpendicular/parallel to the coastline (see Fig. 1).

Nevertheless, E and H polarisation are only two specific cases because, in general, the incident electric field E forms an angle ψ with the coastline (see Fig. 2) so that, in general, one has mixt polarisation.

Thus, in light of this remark, the first basic hypothesis of this work consists of the assumption of mixt polarisation for the source geomagnetic field.

In Figure 2, it is also shown the pipeline layout that is modelled using a broken line along which an abscissa s is defined. At the initial point A, $s = 0$, whereas at the final point, $s = L$, which is the length of the pipeline.

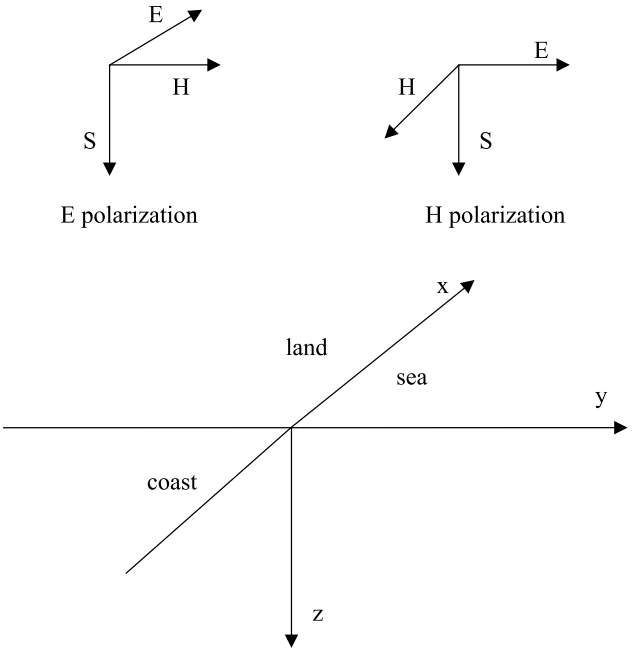

Fig. 1. Scheme of E polarisation (top left) and H polarisation (top right) of a plane wave normally incident on the Earth's surface represented by the xy plane; S is the Poynting vector, and the xy plane represents the land/sea discontinuity.

The second basic assumption is that the conductivity of the earth's layers does not depend on the x coordinate, so a 2D model may be sufficient for PSP and GIC assessment along the pipeline. That may be the case of a long and rectilinear coast (*Weaver, 1994*); a generic section of the earth/sea structure is represented in Fig. 3.

Referencing Figure 3, $\sigma_{i\mathrm{U}}$ and d_{iU} $(i = 1, 2)$ represent the conductivity and the thickness of the first (upper) layer on the land and sea sides, respectively; analogously, $\rho_{i\mathrm{L}}$ and $\mathrm{d}_{i\mathrm{L}}$ $(i = 1, 2)$ represent the resistivity and thickness of the second (lower) layer. Finally, if the mantle is composed of N–2 layers (the last one of infinite depth), ρ_i and d_i $(i = 3, 4, ...N)$ are their resistivity and thickness, respectively.

Figure 3 presents a simple representation of the Earth conductivity structure. We have a first conductive layer, composed of sedimentary rocks or seawater, below which we find the more resistive Earth's crust and, under

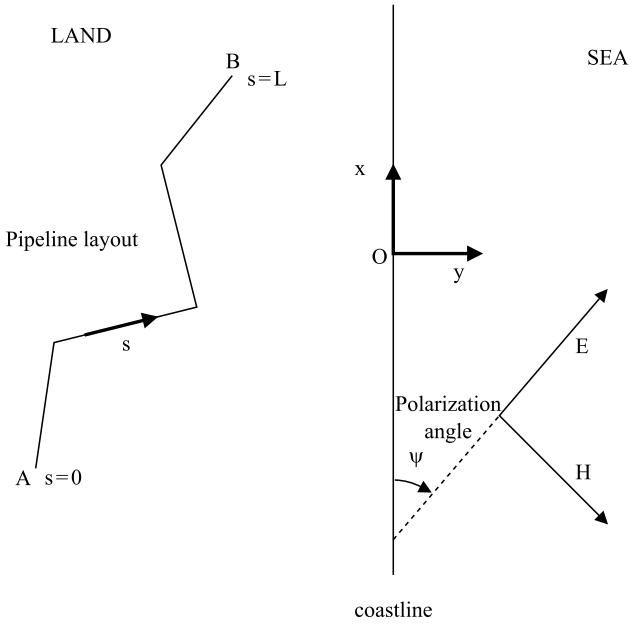

Fig. 2. Definition of the polarisation angle ψ and sketch of the pipeline layout. The quantity s represents the abscissa along the pipeline route; at point A, $s = 0$, whereas at point B, $s = L$, which is the pipeline length.

that, a stratified common basement representing the Earth's mantle.

Nevertheless, it should be noted that the model does not strictly request that the basement structure be common to both sides as represented in Fig. 3; in principle, the modelling allows for different basement structures in the two regions. Anyway, the model is often presented in Fig. 3 and represents a reasonable assumption in many cases.

3. Overview of the calculation method

This section outlines the basic steps of the calculation method using the aid of Fig. 4. Some of these basic steps will be described in more detail in the next sections.

The starting point is the acquisition of the time series data relevant to the inducing geomagnetic field. Subsequently, a forward Fourier transform (Fast Fourier Transform FFT) is used to give the amplitude spectrum of

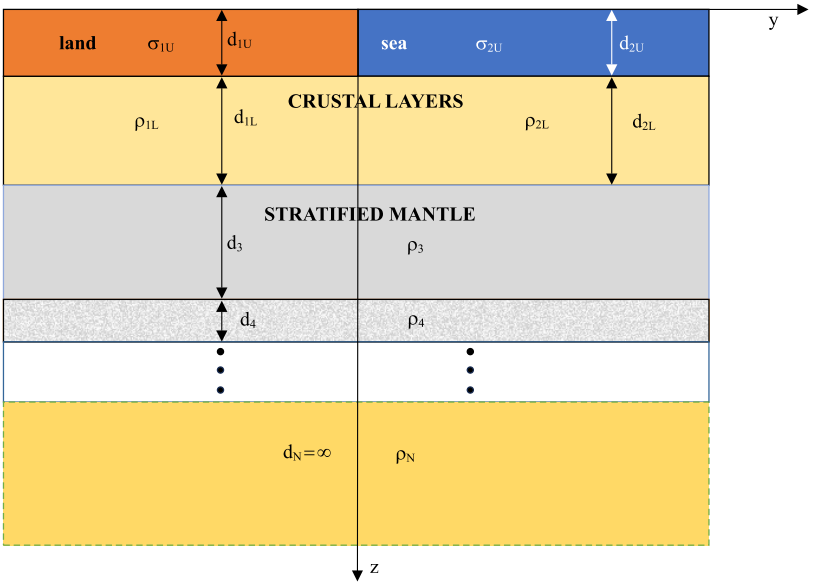

Fig. 3. Model of Earth stratification in proximity of a coastline; the first conductive layer is generally composed of sediments (on the left) and seawater (on the right) below which is the resistive crust and under that is the Earth's mantle.

the geomagnetic field in the frequency domain. Then, multiplying it by the earth surface impedance and by the knowledge of the pipeline layout, one obtains the geoelectric field along the pipeline route, thereby allowing the calculation of the emf generators to be inserted, as active components, in the equivalent circuit representing the induced pipeline under the influence of the geoelectric field.

It is then possible to solve the circuit obtaining the PSP along the pipeline abscissa s in function of the frequency f and of the polarisation angle ψ. A backward Fourier transform (Inverse Fast Fourier Transform IFFT) returns the PSP in function of t, s and ψ.

Nevertheless, we are interested in finding the zones along the pipeline route which are characterised by the largest PSP over the range of different values that can be assumed by the angle ψ. We define these parts along the pipeline route by *riskiest zones*. For this reason, the last step is represented by the construction of the functions that represent the envelopes of maxima and minima for different values of ψ versus the pipeline abscissa s.

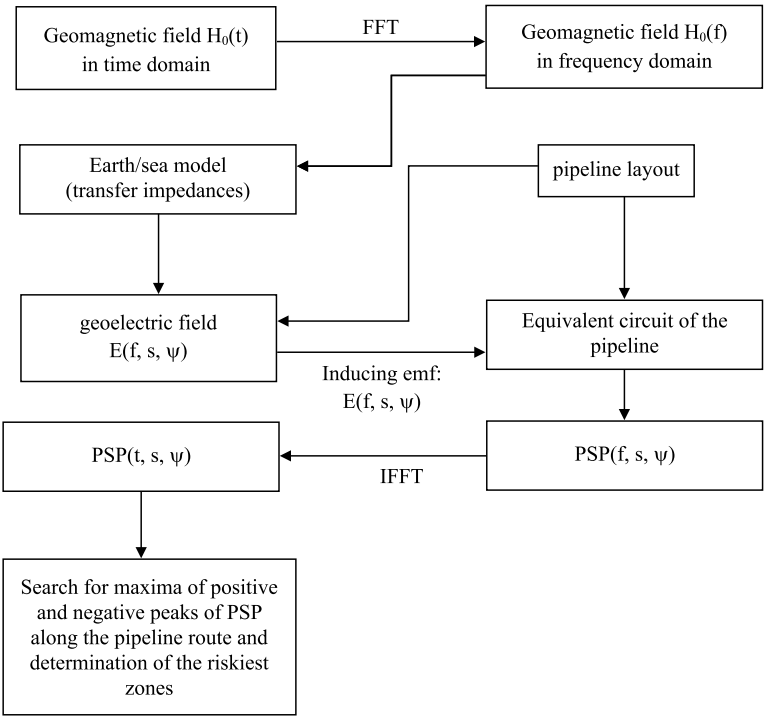

Fig. 4. Block diagram of the main steps involved in the calculation method.

4. Geomagnetic data

As the purpose of our study is to predict the geoelectric field, it is worthwhile to start by adopting a convenient expression that represents the incident magnetic field in the time domain.

Pirjola and Boteler (2017), *Boteler and Pirjola (2019)*, *Boteler et al., (2019)*, *Wang et al. (2021)* adopted a synthetic magnetic field expression in the time domain that can be used as a credible proxy for a real geomagnetic disturbance.

The formula is:

$$\mathrm{H}_0 = \frac{1}{\mu_0} \sum_{m=1}^{7} \left(A_m \sin(2\pi\, f_m\, t + \Phi_m) \right), \tag{1}$$

where μ_0 is the vacuum absolute magnetic permeability, and the quantities A_m, f_m and Φ_m are given in Table 1.

Table 1. Parameters relevant to the synthetic geomagnetic field expression.

m	A_m (nT)	Φ_m (deg)	f_m (Hz)
1	200	10	0.00009259
2	90	20	0.000208333
3	30	30	0.00047619
4	17	40	0.00111111
5	8	50	0.00238095
6	3.5	60	0.00555555
7	1	70	0.0025

We assumed that the incident magnetic field $\mathrm{H}_0(t)$ defined according to Eq. (1) had a duration of three days and the sampling interval was 1 minute (see the plot of $\mathrm{H}_0(t)$ in Fig. 5).

According to *Boteler and Pirjola (2019)*, before taking the Fast Fourier Transform (FFT) of the signal, the time series has been tapered at its ends using a split cosine bell window to prevent spurious frequencies from being introduced by the discontinuities represented by the ends of the time series itself. Finally, to minimise the influence of the tapering on the results of the PSP obtained by the Inverse Fast Fourier Transform (IFFT), it is convenient to limit the analysis only to the central day (i.e. the second day) disregarding the first and third days.

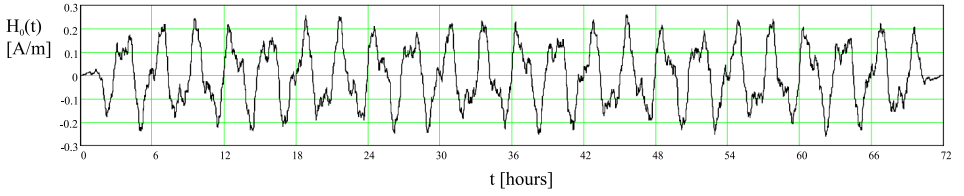

Fig. 5. Plot of the incident geomagnetic field according to Eq. (1) and Table 1. The time series has been tapered, at its ends using a split cosine bell window.

Boteler et al. (2019) observed that the wave shape described by Eq. (1), if amplified by a factor 30, allows the reproduction of the calculated geoelectric field, using the Quebec Earth model, that has been generated

during the, often mentioned in literature, geomagnetic storm of March 13, 1989.

In principle, the calculation method described in this paper can be applied to any time series registration of geomagnetic field. To this aim, it is worthwhile to add that a large amount of real data collected by measurements of magnetic field in the time domain done by many observatories around the world are available at `http://www.intermagnet.org` and `http://supermag.jhuapl.edu`.

5. Geoelectric field

This section presents the relationship existing between the source geomagnetic field H_0 and the induced geoelectric field at the ground surface.

Lucca (2024b) showed that an approximate formula for the geoelectric field as a function of the distance from the coastline y, frequency f and polarisation angle ψ is given by:

$$\vec{E}(y,f,\psi) = E_x(y,f)(\cos\psi)\,\vec{u}_x + E_y(y,f)(-\sin\psi)\,\vec{u}_y\,, \tag{2}$$

where $\vec{u}_x$ and $\vec{u}_y$ are the unit vectors relevant to x and y axes, respectively. The x component of the geoelectric field is given by:

$$E_x(y,f) = \begin{cases} \dfrac{H_0[K_2(f)-K_1(f)]\,\Gamma_2(f)}{\Gamma_2(f)+\Gamma_1(f)}\,\mathrm{e}^{\Gamma_1(f)y} + H_0K_1(f) & y<0 \\ \dfrac{-H_0[K_2(f)-K_1(f)]\,\Gamma_1(f)}{\Gamma_2(f)+\Gamma_1(f)}\,\mathrm{e}^{-\Gamma_2(f)y} + H_0K_2(f) & y>0 \end{cases} \tag{3}$$

with:

$$K_i(f) = \frac{j\omega\mu_0 d_{Li} + Z_{Ti\_3}(f)}{1+\sigma_{iU}d_{iU}[j\omega\mu_0 d_{Li} + Z_{Ti\_3}(f)]} \qquad i=1,2\,, \tag{4}$$

$$\Gamma_i(f) = \sqrt{\frac{j\omega\mu_0}{d_{iU}K_i(f)}} \qquad i=1,2\,,\,, \tag{5}$$

Being, $\omega = 2\pi f$ the angular frequency and $Z_{Ti\_3}(f)$ the surface impedance of the i-th medium "seen" from the interface between the second and the third layer (i.e. the common basement representing the mantle shown in Fig. 3).

The y component of the geoelectric field is given by:

$$E_y(y,f) = \begin{cases} \dfrac{[-\tau_2 Z_{T2}(f) + \tau_1 Z_{T1}(f)]\, H_0}{\sqrt{\tau_1\lambda_1}\left(\frac{\tau_1}{\sqrt{\tau_1\lambda_1}} + \frac{\tau_2}{\sqrt{\tau_2\lambda_2}}\right)} \mathrm{e}^{\frac{y}{\sqrt{\tau_1\lambda_1}}} - Z_{T1}(f)H_0 & y < 0 \\ \dfrac{[-\tau_2 Z_{T2}(f) + \tau_1 Z_{T1}(f)]\, H_0}{\sqrt{\tau_2\lambda_2}\left(\frac{\tau_1}{\sqrt{\tau_1\lambda_1}} + \frac{\tau_2}{\sqrt{\tau_2\lambda_2}}\right)} \mathrm{e}^{\frac{-y}{\sqrt{\tau_2\lambda_2}}} - Z_{T2}(f)H_0 & y > 0 \end{cases} \tag{6}$$

where $\tau_i = \sigma_{iU} d_{iU}$ and $\lambda_i = \rho_{iL} d_{iL}$ $(i = 1, 2)$ while Z_{Ti} is the surface impedance relevant to the stratified medium (land or sea) evaluated very far from the discontinuity so that its effect can be considered negligible; explicit formulas for calculating the surface impedance Z_{Ti}, using a recursive relation, are given by *Trichtchenko and Boteler (2002)*.

6. Equivalent circuit of the pipeline

As already mentioned, and as depicted in Fig. 6, the influence of the geomagnetic field on the pipeline can be studied by an equivalent circuit composed by a chain of a suitable number N of elementary Pi circuits also said cells; each cell has passive elements given by the impedance Z and admittance

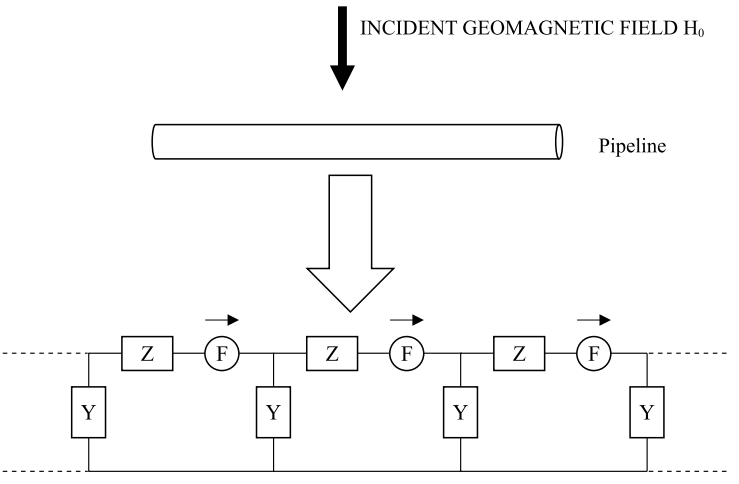

Fig. 6. Schematic representation of the pipeline equivalent circuit under the influence of a geomagnetic field.

Y that, due to the extremely low frequencies involved in the phenomenon (typically the range is [0.1 mHz, 100 mHz]) can be considered DC (Direct Current) parameters (i.e. resistance and conductance).

Regarding the active elements, i.e. the emf generators F applied to each cell, they are strictly related to the geoelectric field and the orientation of the pipeline layout with respect to the coastline through the angle $\theta = \theta(s)$ (orientation angle) that depends on the pipeline abscissa s. See Fig. 7.

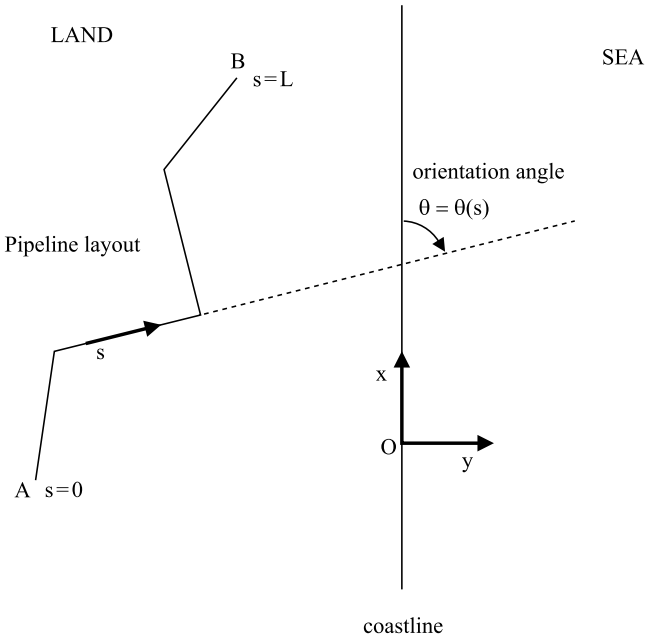

Fig. 7. Pipeline layout and definition of the orientation angle θ formed with the coastline; this angle is not constant but depends on the pipeline abscissa s.

To calculate the elementary emf generator $\mathrm{d}F$ induced along the generic infinitesimal element of pipeline layout $\vec{\mathrm{d}s}$, we first define it by:

$$\vec{\mathrm{d}s} = \cos(\theta(s))\,\mathrm{d}s\,\vec{u}_x + \sin(\theta(s))\,\mathrm{d}s\,\vec{u}_y\,, \tag{7}$$

where $\vec{u}_x$ and $\vec{u}_y$ are the unit vectors relevant to the x and y axes, respectively.

By remembering that $\mathrm{d}F(s)$ is the scalar product of the electric field (given by Eq. (2)) and $\vec{\mathrm{d}s}$, one has:

$$\mathrm{d}F(s) = E_x(y(s), f)\,\cos(\theta(s))\mathrm{d}s + E_y(y(s), f)\,(-\sin\psi\sin(\theta(s)))\mathrm{d}s\,. \tag{8}$$

Notice from Eq. (8) that if the entire layout of the pipeline is parallel/perpendicular to the coastline, only the E/H polarised component of the electric field contributes to the inducing emf.

If the generic i-th cell, of length L_i, is defined between the abscissas s_i and s_{i+1}, the total emf F_i is given by:

$$F_i = \int_s^{s_{i+1}} [E_x(y(s), f)\cos\psi\cos(\theta(s)) + E_y(y(s), f)(-\sin\psi\sin(\theta(s)))]\,\mathrm{d}s \qquad i = 1, 2, ..., N. \tag{9}$$

To simplify the notation, we omit the dependence on the frequency f in the formulas below.

By substituting formulas (3) and (6) into (9) and after integration one has:

$$F_i = F1_i + F2_i + F3_i + F4_i\,, \tag{10}$$

where:

$$F1_i = \left(\frac{H_0(K_2 - K_1)\Gamma_2}{\Gamma_1 + \Gamma_2}\,\mathrm{e}^{\Gamma_1 Y_i}\cos\psi(X_{i+1} - X_i)\right) \times \times \frac{\mathrm{e}^{\Gamma_1 \frac{Y_{i+1} - Y_i}{L_i} s_i}}{(Y_{i+1} - Y_i)\Gamma_1}\left(\mathrm{e}^{\Gamma_1(Y_{i+1} - Y_i)} - 1\right), \tag{11}$$

$$F2_i = H_0 K_1 \cos\psi(X_{i+1} - X_i)\,, \tag{12}$$

$$F3_i = \left[\frac{(-\tau_2 Z_{T2} + \tau_1 Z_{T1})H_0\,\mathrm{e}^{\frac{Y_i}{\sqrt{\tau_1\lambda_1}}}}{\frac{\tau_1}{\sqrt{\tau_1\lambda_1}} + \frac{\tau_2}{\sqrt{\tau_2\lambda_2}}}\,(-\sin\psi)\,\mathrm{e}^{\frac{(Y_{i+1} - Y_i)s_i}{L_i\sqrt{\tau_1\lambda_1}}}\right] \times \times \left[\mathrm{e}^{\frac{(Y_{i+1} - Y_i)}{\sqrt{\tau_1\lambda_1}}} - 1\right], \tag{13}$$

$$F4_i = -Z_{T1}H_0(-\sin\psi)(Y_{i+1} - Y_i)\,. \tag{14}$$

In formulas (11)–(14) (valid only if the pipeline is located in the onshore region i.e. for $y < 0$), the quantities $(X_i Y_i)$ and $(X_{i+1} Y_{i+1})$ represent the initial and final coordinates of the i-th cell along the pipeline route.

It is useful to note that when the pipeline is located far from the coast, the quantities $F1_i$ and $F3_i$ vanish meaning that the geoelectric coast effect is negligible; thus, the remaining terms $F2_i$ and $F4_i$ describe the influence on the pipeline that would exist in the absence of the land-sea discontinuity.

As far as the detailed description of the algorithm for solving the equivalent circuit of the pipeline is concerned, one may consider the previously quoted literature or refer to *Lucca (2024a)*; for brevity reasons we omit this part in the present paper.

The solution of the equivalent circuit of the pipeline gives us potential and current (i.e. PSP and GIC) in function of the pipeline abscissa s, of the frequency f and of the polarisation angle ψ. The PSP calculation must be repeated for all frequencies present in the spectrum of the driving geomagnetic field $H_0(t)$, and finally, a backward Fourier transform (Inverse Fast Fourier Transform IFFT) returns the PSP as a function of s, t and ψ.

Notice, from Equation (9), that a change of the polarisation angle from the generic value ψ to the value $\psi+180°$ implies a change in the sign of the driving emf which, in turn, means, in the time domain, a reversal polarity for PSP and GIC with no change in modulus. For such a reason, in the following, we shall consider only the interval $[0°, 180°]$ for the variable ψ.

7. Riskiest zones along the pipeline route

Even if the knowledge of the PSP as a function of pipeline abscissa s, time t and polarisation angle ψ gives us complete information about the impact of the geomagnetic field, we are interested in determining the zones along the pipeline route that are potentially most influenced during the occurrence of a geomagnetic storm.

To achieve this goal, it is useful to consider the functions $\Omega^+ = \Omega^+(s, \psi)$ and $\Omega^- = \Omega^-(s, \psi)$ that represent the envelopes of the positive and negative peaks assumed by the PSP in function of s and ψ. Nevertheless, as the polarisation angle has a significant influence on the induced PSP, it is worthwhile to find, for any given value of s, the maximum of the function $\Omega^+(s, \psi)$ evaluated in the range of interest for ψ that is the interval $[0°, 180°]$ thus obtaining the function $\xi^+_{max} = \xi^+_{max}(s)$; in other words, $\xi^+_{max}(s)$ represents the maximum value among the positive peaks for a given abscissa s in the range $[0°, 180°]$ for the polarisation angle ψ.

Moreover, by considering the same given value for s and the same interval $[0°, 180°]$ for ψ, it is also convenient to find the minimum of $\Omega^+(s, \psi)$ so obtaining the function $\xi^+_{min} = \xi^+_{min}(s)$; in other words, $\xi^+_{min}(s)$ represents the minimum value among the positive peaks for a given abscissa s in the range $[0°, 180°]$ for the polarisation angle ψ. In such a way, the difference $\Delta^+(s) = \xi^+_{max}(s) - \xi^+_{min}(s)$ represents the range of variability related to the positive peaks; by plotting $\Delta^+(s)$ (see section 8) one obtains a kind of strip having variable width in function of s, which represents, for any given value of the pipeline abscissa, the range of all the possible values that can be assumed by the positive peaks of PSP by varying the polarisation angle ψ.

In an analogous way, one can define, for the negative peaks, the function $\Delta^-(s) = \xi^-_{min}(s) - \xi^-_{max}(s)$.

By studying the trend of the functions $\xi^+_{max}(s)$ together with $\Delta^+(s)$ for the positive peaks and $\xi^-_{min}(s)$ together with $\Delta^-(s)$ for the negative peaks, one can determine the riskiest zones along the pipeline route and, at the same time, the range of variability related to these results.

8. Example of an application

To illustrate the calculation method presented in the previous sections, let us consider a pipeline with a length of about 37.5 km whose layout, represented by a broken line, is shown in Fig. 8. The minimum distance of the pipeline layout from the coastline (point A) is 1 km; the pipeline is grounded at point A with grounding resistance $R_g = 5\,\Omega$ while at point B, there is no grounding point; this grounding resistance is typically related to the anode used for the CP of the pipeline. The values of the per unit length pipe resistance and conductance are 0.0049 Ω/km and 0.0096 S/km, respectively; the pipeline layout is discretized by 155 cells that, in general, have different lengths, and the maximum length is 500 m.

The data relevant to the earth/sea stratification model adopted are shown in Table 2, and they are mostly based on the ones presented in *Chakraborty et al. (2022)* and *Boteler et al. (2024)*.

As for the source geomagnetic field, we assume that its magnitude is expressed by Eq. (1).

Figure 9 shows, as an example, the PSP as a function of the time evaluated at four different points along the pipeline and for a polarisation angle

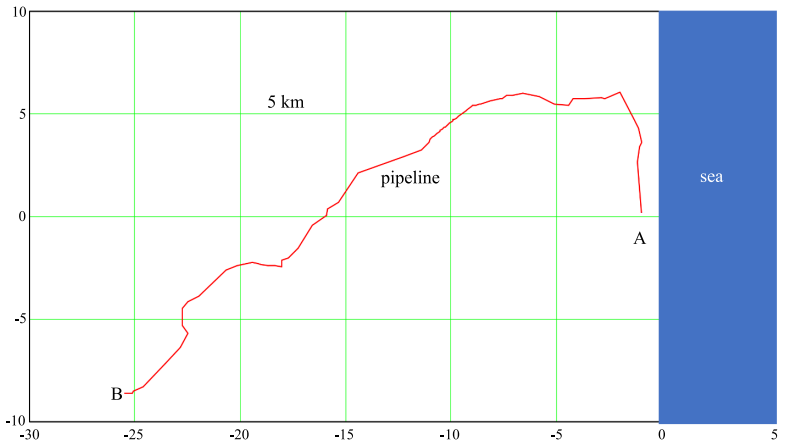

Fig. 8. Sketch of the pipeline layout showing the discontinuity sea/land.

$\psi = 30°$. We can notice that the magnitude of the PSP fluctuations (characterised by positive and negative peaks) strongly depends on the pipeline abscissa, and the largest values are found at the not grounded extremity (that is, point B in Fig. 8, $s = 37.5$ km); in contrast they are very small for $s = 10$ km, which is in a more central part of the pipeline route, confirming the results of theory and experience (*Boteler and Seager, 1998*).

In Figure 10, the plots of the envelopes of the positive peaks $\Omega^+(s, \psi)$ for different values of ψ are drawn (the envelopes of negative peaks are just symmetrical with respect to the abscissa axis, so they have not been plotted); the graphs show the significant influence of the polarisation angle

Table 2. Data relevant to the earth/sea stratification model.

Land side			**Sea side**		
Description	d **(km)**	ρ **(Ωm)**	**Description**	d **(km)**	ρ **(Ωm)**
sediments	0.05	50	seawater	0.2	0.3
crust	30	3000	crust	29.85	3000
mantle lithosphere	140	10000	mantle lithosphere	140	10000
upper mantle	247	100	upper mantle	247	100
transition zone	250	10	transition zone	250	10
lower mantle	∞	1	lower mantle	∞	1

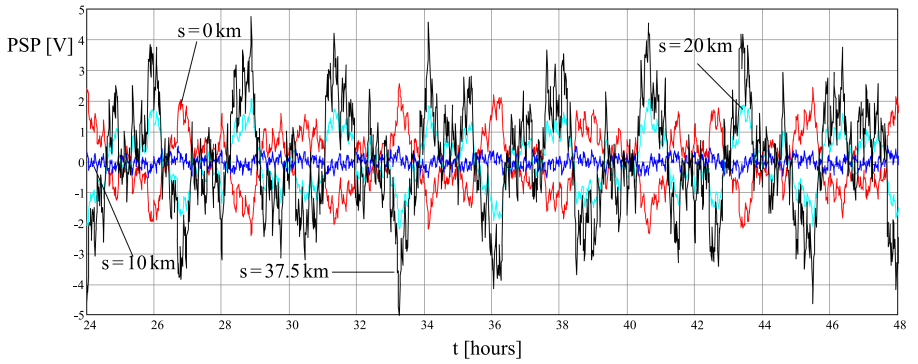

Fig. 9. PSP in function of time evaluated during the central day of a three-day storm; the potential has been calculated at different points along the pipeline under the hypothesis that $\psi = 30°$.

and we can notice that, for most of the pipeline route, the worst case is in correspondence of $\psi = 90°$ (pure H polarisation) while the best case is in correspondence of $\psi = 0°$ (pure E polarisation).

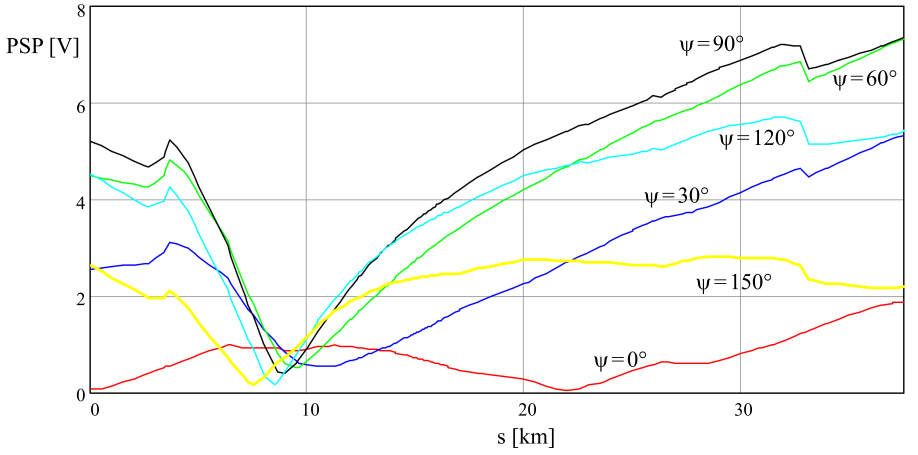

Fig. 10. Envelopes of the positive peaks of PSP $\Omega^+(s, \psi)$ versus pipeline abscissa for different values of polarisation angle ψ.

In Figure 11, we plot the functions $\xi^+_{max}(s)$ and $\xi^+_{min}(s)$ evaluated in the range $[0°, 180°]$ for the polarisation angle ψ and by considering three different values for the grounding resistance R_g that is: 1 Ω, 5 Ω and 10 Ω; we remind that their difference defines $\Delta^+(s)$ i.e. the range of variability

of the positive peaks in function of the pipeline abscissa s. In this case, the corresponding negative functions are symmetrical with respect to the abscissa axis so they are not drawn.

In the plots, we considered two cases: the first one considering the geoelectric coast effect and the second neglecting it; the reason is to have an idea of the importance of this effect in the evaluation of the PSP along the pipeline.

In Figure 12, the same holds as for Fig. 11 except for the position of the grounding point, which is in B instead of A.

Both figures show:

- the importance of considering the coast effect in the model; in fact, the results are very different when considering it or not; the inclusion of the coast effect yields results that are significantly larger than the ones relevant to the simpler case where the discontinuity sea-land does not exist;
- the importance of the value of the grounding resistance; indeed, by increasing the value of R_g the values of ξ^+_{max} and Δ^+ tend to increase at the grounded side of the pipeline route, whereas they tend to decrease at the not grounded side;
- the importance of the location of the grounding resistance; indeed, we can notice a greater influence on the shape of the curves representing ξ^+_{max} and Δ^+ when the grounding point is placed in A (nearer to the coast) instead of B (farther from the coast).

In Figure 13, we have drawn the plots by considering three different values for the sea depth, grounding point in B and $R_g = 5\ \Omega$. As specified in Section 2, the generalised thin sheet model cannot be applied to very deep seas (depth less than 1000 m), so we considered depths of 200, 400 and 800 m; the plots in Fig. 13 show that the influence of this parameter is small.

Figure 10 shows that the H polarised component of the geoelectric is dominant with respect to the E polarised one; from Eq. (6) we can notice that it exponentially attenuates according to the attenuation constant given by $(\tau_1\lambda_1)^{-1/2} = (\sigma_{1U}d_{1U}\rho_{1L}d_{1L})^{-1/2}$. Thus, to have an idea of the geoelectric coast effect attenuation versus distance from the coastline, it is useful to define, according to *Ranganayaki and Madden (1980)*, the adjustment

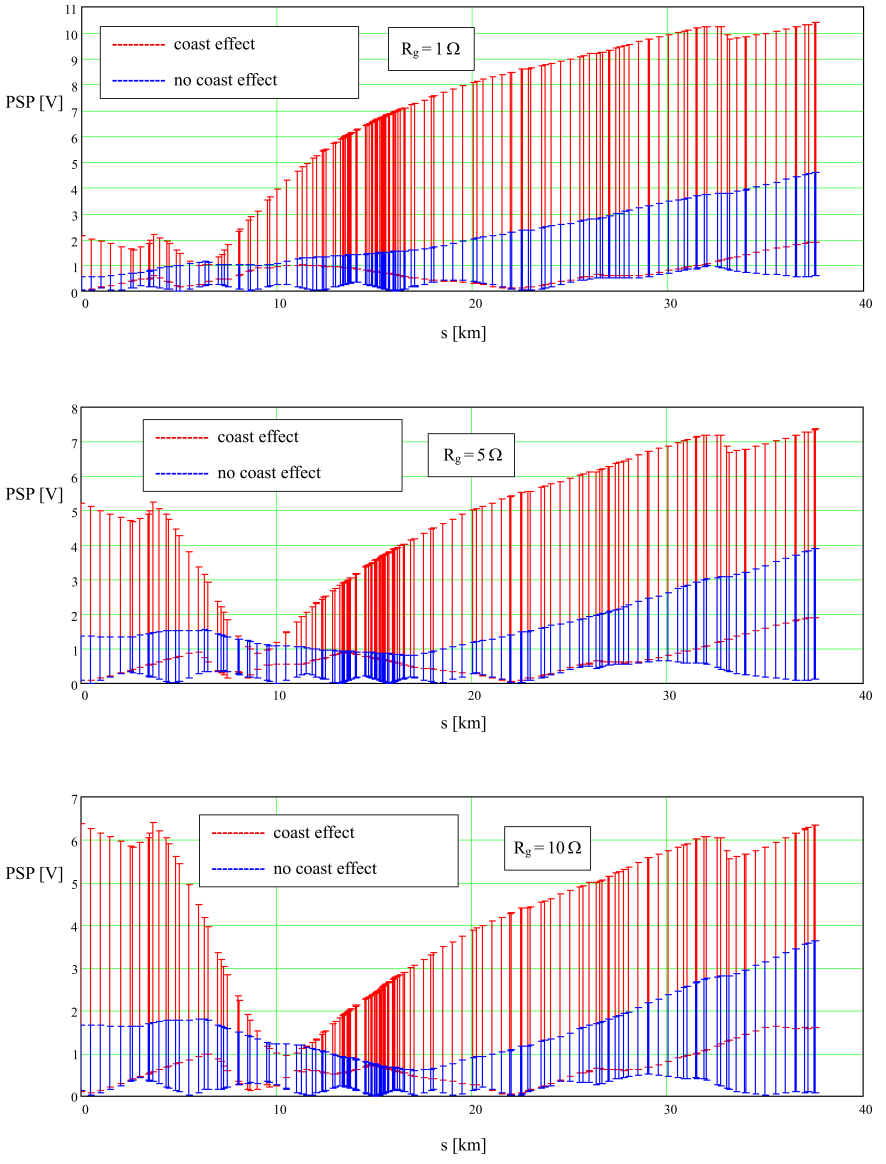

Fig. 11. Range of variability for positive peak values of PSP versus pipeline abscissa evaluated in the interval $[0°, 180°]$ for the polarisation angle ψ; grounding point in A. Minimum distance of the pipeline layout from the coastline 1000 m.

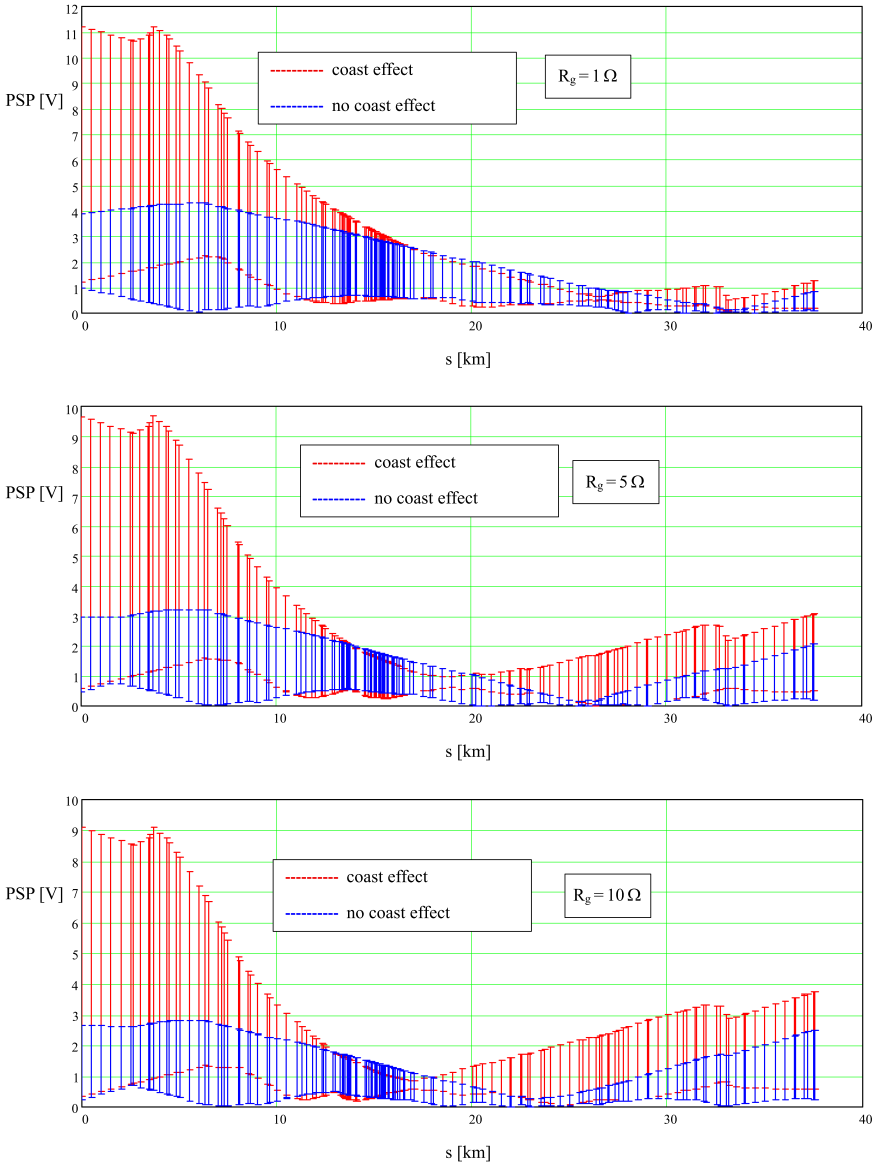

Fig. 12. Range of variability for positive peak values of PSP versus pipeline abscissa evaluated in the interval $[0°, 180°]$ for the polarisation angle ψ; grounding point in B. Minimum distance of the pipeline layout from the coastline 1000 m.

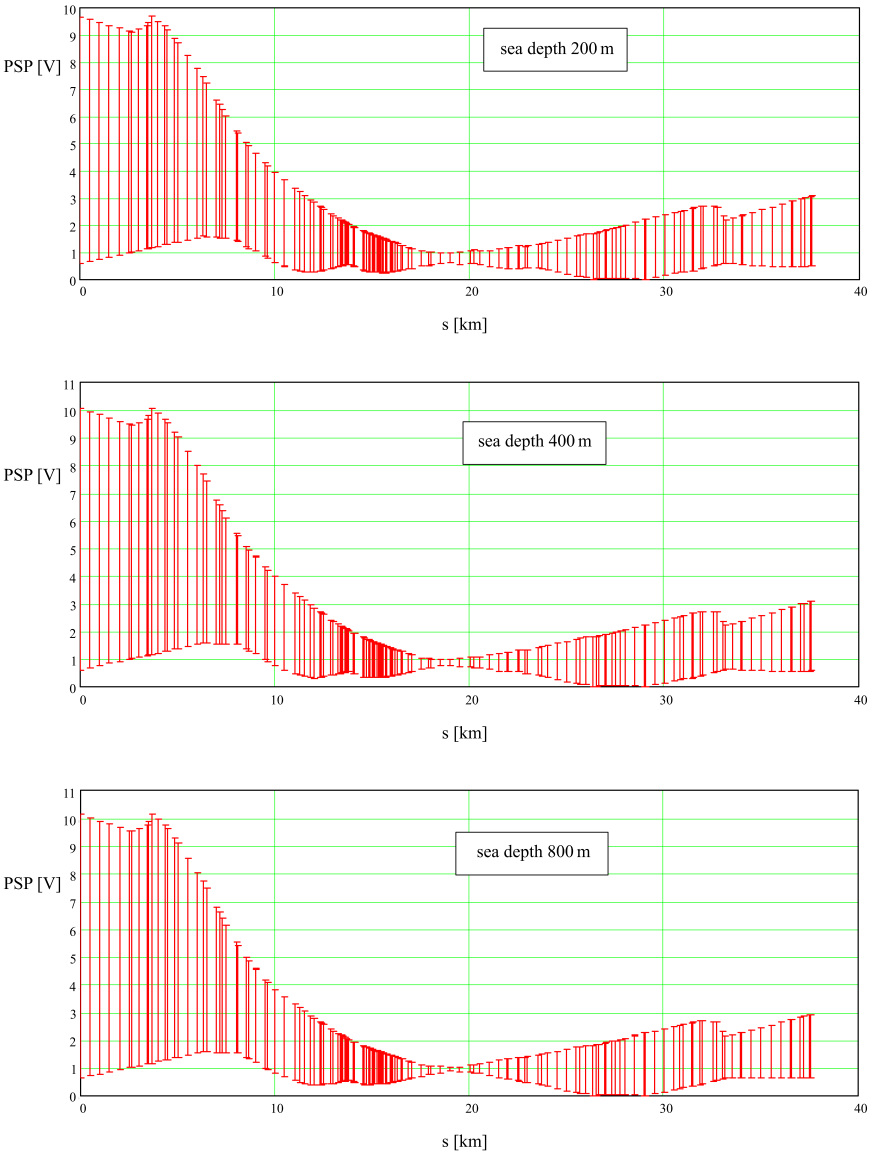

Fig. 13. Range of variability for positive peak values of PSP versus pipeline abscissa evaluated in the interval $[0°, 180°]$ for the polarisation angle ψ; grounding point in B with $R_g = 5\ \Omega$. Evaluation by considering three different values for sea depth. Minimum distance of the pipeline layout from the coastline 1000 m.

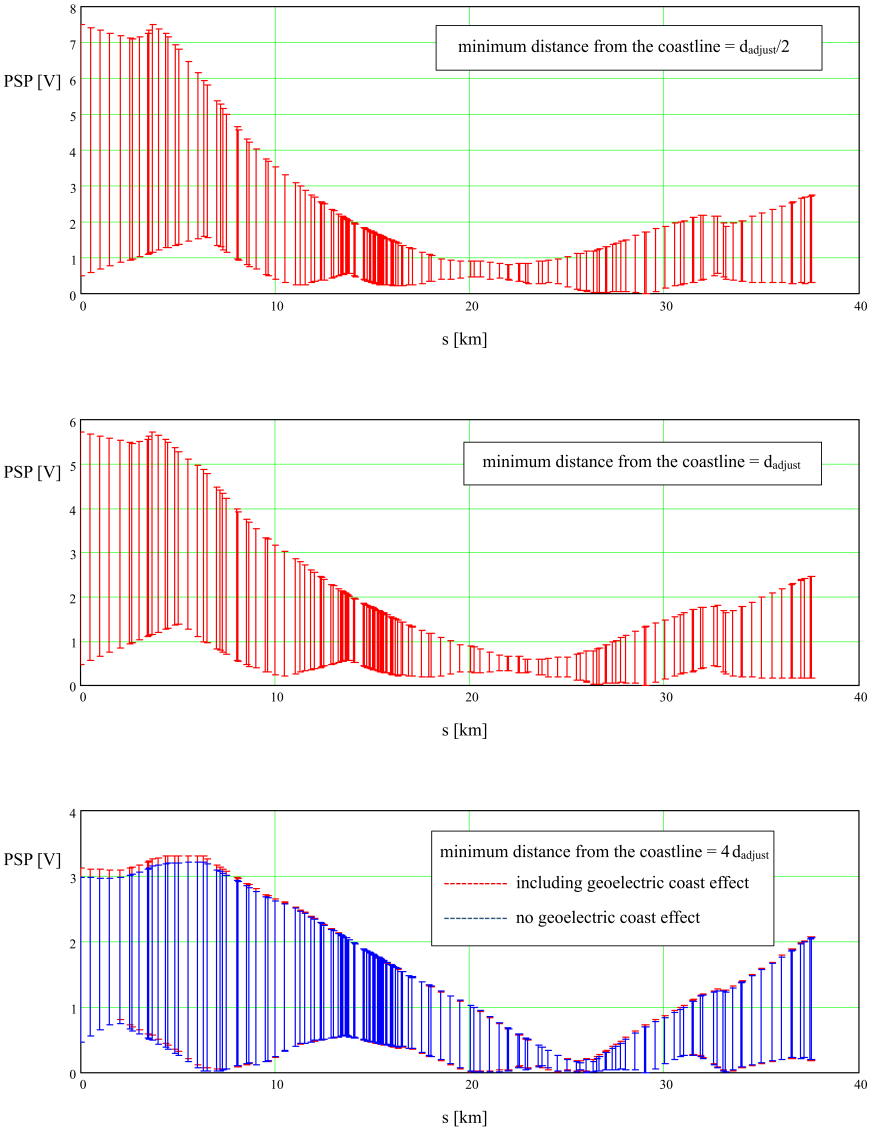

Fig. 14. Range of variability for positive peak values of PSP versus pipeline abscissa evaluated in the interval $[0°, 180°]$ for the polarisation angle ψ; grounding point in B with $R_g = 5\ \Omega$. Evaluation by considering three different values of distance of the pipeline from the coast; $d_{\mathrm{adjust}} = 6708$ m.

distance $d_{\text{adjust}} = (\sigma_{1U} d_{1U} \rho_{1L} d_{1L})^{1/2}$ that, as we can see, is proportional to the characteristics of the first two earth layers on the land side. Therefore, if one wants to quantify the influence of the minimum distance of the pipeline layout from the coast, it is useful to express it in terms of multiples or submultiples of d_{adjust}.

Figure 14 shows the variability range for positive peaks of PSP for different values of pipeline distance from the coastline. As one can expect, by increasing the distance from the coastline, the values of PSP decrease and so does the range of variability; in particular, when the minimum distance from the coastline is equal to $4d_{\text{adjust}}$ the coast effect can be considered negligible (bottom plot in Fig. 14). In fact, in that case, the results obtained by including the coast effect (red) and those ignoring it (blue) are almost coincident.

9. Conclusions

In this paper, we present a calculation method for evaluating the potential along a pipeline located in proximity of a coastline under the influence of a geomagnetic storm. The peculiarity of this algorithm is the inclusion of the geoelectric coast effect in modelling the lumped emf generators that play the role of active elements in the equivalent electric circuit describing the pipeline.

This method allows for the determination of the riskiest zones (that is, the ones subjected to the largest PSP) along the pipeline route by considering the whole range of variability of the polarisation angle of the inducing geomagnetic field that is not *a priori* known and is one of the most influencing parameters involved in the phenomenon.

The first point to be noted is that neglecting the coast effect yields a significant underestimation of the results.

Further analyses have also shown that the extension and position of the riskiest zones are strongly influenced by:

- the value of the pipeline grounding resistance;
- the position of the pipeline grounding resistance;
- the ratio between the minimum distance of the pipeline from the coast and the adjustment distance.

We further add that:

- the sea depth (for values less than 1000 m) has little influence on the results;
- when the ratio between the minimum distance of the pipeline from the coast and the adjustment distance is greater than 4, the geoelectric coast effect can be neglected.

This calculation method can be a useful tool, also at the design stage of a new pipeline, that allows individuating the most exposed zones, along the pipeline layout to the risk of high geoelectric potentials. This information can be an aid in preparing specific countermeasures to minimise the threaten represented by geomagnetic storms.

Acknowledgements. The author gratefully thanks the anonymous referees for their comments and suggestions that allowed us to improve the paper.

References

Boteler D. H., 1994: Geomagnetically induced currents: present knowledge and future research. IEEE Trans. Power Del., **9**, 1, 50–58, doi: 10.1109/61.277679.

Boteler D. H., 2000: Geomagnetic effects on the pipe-to-soil potentials of a continental pipeline. Adv. Space Res., **26**, 1, 15–20, doi: 10.1016/S0273-1177(99)01020-0.

Boteler D. H., 2003: Geomagnetic Hazards to Conducting Networks. Nat. Hazards, **28**, 2–3, 537–561, doi: 10.1023/A:1022902713136.

Boteler D. H., 2013: A new versatile method for modelling geomagnetic induction in pipelines. Geophys. J. Int., **193**, 1, 98–109, doi: 10.1093/gji/ggs113.

Boteler D. H., Seager W. H., 1998: Telluric Currents: A Meeting of Theory and Observation. Corrosion, **54**, 9, 751–755, doi: 10.5006/1.3284894.

Boteler D. H., Trichtchenko L., Edwall H.-E., 2013: Telluric Effects on Pipelines. In: Proc. CEOCOR International Congress and Technical Exhibition, June 6–7, 2013, Florence, Italy.

Boteler D. H., Pirjola R. J., 2019: Numerical Calculation of Geoelectric Fields That Affect Critical Infrastructure. Int. J. Geosci., **10**, 10, 930–949, doi: 10.4236/ijg.2019.10 10053.

Boteler D. H., Pirjola R. J., Marti L., 2019: Analytic Calculation of Geoelectric Fields Due to Geomagnetic Disturbances: A Test Case. IEEE Access, **7**, 147029–147037, doi: 10.1109/ACCESS.2019.2945530.

Boteler D. H., Chakraborty S., Shi X., Hartinger M. D., Wang X., 2024: An Examination of Geomagnetic Induction in Submarine Cables. Space Weather, **22**, 2, e2023SW003687, doi: 10.1029/2023SW003687.

Chakraborty S., Boteler D. H., Shi X., Murphy B. S., Hartinger M. D., Wang X., Lucas G., Baker J. B. H., 2022: Modeling geomagnetic induction in submarine cables. Front. Phys., **10**, 1022475, doi: 10.3389/fphy.2022.1022475.

de Moraes J. F., Paulino I., Alves L. R., Denardini C. M., 2020: Evaluation of possible corrosion enhancement due to telluric currents: case study of the Bolivia–Brazil pipeline. Ann. Geophys., **38**, 4, 881–888, doi: 10.5194/angeo-38-881-2020.

Divett T., Ingham M., Richardson G., Sigley M., Rodger C. J., 2023: Modeling Pipe to Soil Potentials from Geomagnetic Storms in Gas Pipelines in New Zealand. Space Weather, **21**, 12, doi: 10.1029/2023SW003601.

Dong B., Wang Z., Boteler D., Pirjola R., 2013: Review of earth conductivity modelling for calculating geo-electric fields. In: Proc. 2013 IEEE Power & Energy Society General Meeting, 21–25 July 2013, Vancouver BC, doi: 10.1109/PESMG.2013.6672216.

Gummow R. A., Boteler D. H., Trichtchenko L., 2002: Telluric and Ocean Current Effects on Buried Pipelines and Their Cathodic Protection Systems. Pipeline Research Council, Technical Report L51909, PRCI.

Liu C., Wang X., Lin C., Song J., 2019a: Proximity Effects of Lateral Conductivity Variations on Geomagnetically Induced Electric Fields. IEEE Access, **7**, 6240–6248, doi: 10.1109/ACCESS.2018.2889461.

Liu C., Wang X., Zhang S., Xie C., 2019b: Effects of Lateral Conductivity Variations on Geomagnetically Induced Currents: H-Polarization. IEEE Access, **7**, 6310–6318, doi: 10.1109/ACCESS.2018.2889462.

Liu M., 2024: Study on Modeling and Efficient Algorithms for Geomagnetic Induction in AC Transmission Grids and Gas Pipeline Networks. Ph.D. Thesis, Politecnico di Torino and Xi'an Jiaotong University, available online at https://iris.polito.it/handle/11583/2991366.

Liu M., Xie Y., Dong N., Wang Z., Yang Y., 2022: Numerical Analysis of Nonuniform Geoelectric Field Impacts on Geomagnetic Induction in Pipeline Networks. IEEE Transactions on Electromagnetic Compatibility, **64**, 4, 999–1009, doi: 10.1109/TEMC.2022.3158885.

Lucca G., 2016: Electromagnetic interference from power lines on pipelines: influence of pipe insulating coating degradation. Int. Trans. Electr. Energ. Syst., **26**, 12, 2699–2712, doi: 10.1002/etep.2229.

Lucca G., 2024a: Geomagnetically induced potential on pipelines: A probabilistic approach. Adv. Space Res., **73**, 6, 3060–3068, doi: 10.1016/j.asr.2023.12.043.

Lucca G., 2024b: Induced geoelectric field: influence of polarization in coast effect and proximity effect. Ann. Geophys., **67**, 5, SA549, doi: 10.4401/ag-9107.

McKay A. J., 2003: Geoelectric Fields and Geomagnetically Induced Currents in the United Kingdom. Ph.D. Thesis, University of Edinburgh, Scotland, UK, available online at http://hdl.handle.net/1842/639.

Pilipenko V. A., 2021: Space weather impact on ground-based technological systems. Solar-Terr. Phys., **7**, 3, 68–104, doi: 10.12737/stp-73202106.

Pirjola R. J., Boteler D. H., 2017: Truncation of the Earth Impulse Responses Relating Geoelectric Fields and Geomagnetic Field Variations. Geosci. Res., **2**, 2, 72–92, doi: 10.22606/gr.2017.22002.

Pulkkinen A.,Pirjola R., Boteler D., Viljanen A., Yegorov I., 2001: Modelling of space weather effects on pipelines. J. Appl. Geophys., **48**, 4, 233–256, doi: 10.1016/S0926-9851(01)00109-4.

Ranganayaki R. P., Madden T. R., 1980: Generalized thin sheet analysis in magnetotellurics: an extension of Price's analysis. Geophys. J. Int., **60**, 3, 445–457, doi: 10.1111/j.1365-246X.1980.tb04820.x.

Trichtchenko L., Boteler D. H., 2002: Modelling of geomagnetic induction in pipelines. Ann. Geophys., **20**, 7, 1063–1072, doi: 10.5194/angeo-20-1063-2002.

Trichtchenko L., Trishchenko A. P., Hejda P., Langer R., 2023: Evaluation of telluric-associated corrosion on buried pipelines. J. Atmos. Sol.-Terr. Phys., **248**, 106082, doi: 10.1016/j.jastp.2023.106082.

von Baeckmann W., Schwenk W., Prinz W. (Eds.), 1997: Handbook of Cathodic Corrosion Protection: Theory and Practice of Electrochemical Protection Processes (3rd ed.). Houston, Texas, Gulf Pub. Co., 567 p.

Wang X., Liu C., Kang Z., 2021: Effect of the Earth's lateral conductivity variations on geomagnetically induced currents in power grids. Int. J. Electr. Power Energy Syst., **132**, 107148, doi: 10.1016/j.ijepes.2021.107148.

Wang X., Boteler D. H., Pirjola R. J., 2023: Distributed-Source Transmission Line Theory for Modeling the Coast Effect on Geoelectric Fields. IEEE Trans. Power Del., **38**, 5, 3541–3550, doi: 10.1109/TPWRD.2023.3279462.

Weaver J. T., 1994: Mathematical Methods for Geo-Electromagnetic Induction. Research Studies Press, Taunton, England, 316 p.